Published in final edited form as:
Proc SPIE. 2013 February 26; 8584: . doi:10.1117/12.2004931.

Numerical 3D modeling of heat transfer in human tissues for microwave radiometry monitoring of brown fat metabolism

Dario B. Rodrigues[*,a,b], **Paolo F. Maccarini**[a], **Sara Salahi**[c], **Erin Colebeck**[d], **Erdem Topsakal**[d], **Pedro J. S. Pereira**[b,e], **Paulo Limão-Vieira**[b], and **Paul R. Stauffer**[a]

[a]Department of Radiation Oncology, Hyperthermia Division, PO BOX 3085 Duke University Medical Center, Durham, NC 27710, USA

[b]CEFITEC, Departamento de Física, Faculdade de Ciências e Tecnologia, Universidade Nova de Lisboa, 2829-516 Caparica, Portugal

[c]ANSYS, Inc., California, USA

[d]Department of Electrical and Computer Engineering, Mississippi State University, Mississippi State, MS 39762, USA

[e]Departament of Mathematics, Instituto Superior de Engenharia de Lisboa, Rua Conselheiro Emídio Navarro 1, 1959-007 Lisboa, Portugal

Abstract

Background—Brown adipose tissue (BAT) plays an important role in whole body metabolism and could potentially mediate weight gain and insulin sensitivity. Although some imaging techniques allow BAT detection, there are currently no viable methods for continuous acquisition of BAT energy expenditure. We present a non-invasive technique for long term monitoring of BAT metabolism using microwave radiometry.

Methods—A multilayer 3D computational model was created in HFSS™ with 1.5 mm skin, 3–10 mm subcutaneous fat, 200 mm muscle and a BAT region (2–6 cm^3) located between fat and muscle. Based on this model, a log-spiral antenna was designed and optimized to maximize reception of thermal emissions from the target (BAT). The power absorption patterns calculated in HFSS™ were combined with simulated thermal distributions computed in COMSOL® to predict radiometric signal measured from an ultra-low-noise microwave radiometer. The power received by the antenna was characterized as a function of different levels of BAT metabolism under cold and noradrenergic stimulation.

Results—The optimized frequency band was 1.5–2.2 GHz, with averaged antenna efficiency of 19%. The simulated power received by the radiometric antenna increased 2–9 mdBm (noradrenergic stimulus) and 4–15 mdBm (cold stimulus) corresponding to increased 15-fold BAT metabolism.

Conclusions—Results demonstrated the ability to detect thermal radiation from small volumes (2–6 cm^3) of BAT located up to 12 mm deep and to monitor small changes (0.5 °C) in BAT metabolism. As such, the developed miniature radiometric antenna sensor appears suitable for non-invasive long term monitoring of BAT metabolism.

[*]db.rodrigues@campus.fct.unl.pt; phone 919-668-1980.

Keywords

Brown fat metabolism; microwave radiometry; 3D multiphysics modeling; noninvasive monitoring; log spiral antenna

1. INTRODUCTION

Mammals have two functionally different types of adipose tissue: white fat and brown fat. White adipose tissue (WAT) stores excess energy and releases hormones that tend to lower whole-body metabolism and promote insulin resistance. Obesity results from excess accumulation of WAT due to long term imbalance between energy intake and expenditure [1]. In contrast to WAT, brown adipose tissue (BAT) metabolizes fat to generate heat when stimulated [2]. The thermogenesis process associated with BAT can be a substantial portion of the body's resting heat generation. Thus the ability to stimulate BAT activity may help mediate weight gain and insulin sensitivity [3].

In spite of its potential significance in controlling obesity and diabetes, there are few viable methods to locate and quantify BAT activity in humans. Positron-emission tomography (PET) and PET/CT have proven most effective for locating BAT due to its high uptake of 18F-FDG [4–6]. These studies are expensive however and risks associated with radiation exposure prevent repetitive scanning. Magnetic Resonance Imaging (MRI) has also been used but is similarly expensive and poorly-suited to repetitive scan investigations [2, 7]. Infrared thermography is a passive approach that has demonstrated feasibility in locating BAT by detecting the increased metabolic activity from conduction of locally increased temperature at depth to the skin surface [8]. In a recent study with cold exposure (17°C for 30 min), the supraclavicular skin temperature reduced by just 0.9 °C, in contrast to a reduction of 2.0 °C in the mediastinum, indicating presence of active brown fat in the supraclavicular region [9]. Conclusions of these studies were that infrared thermal imaging was useful for detecting BAT but was not sufficiently sensitive to quantify small changes in thermogenesis of subsurface BAT since it is particularly affected by blood flow of underlying tissues and environmental conditions. All three imaging techniques are logistically unsuited to continuously track BAT activity over a long period of time.

In order to facilitate studies of BAT metabolism that might lead to new approaches in control of obesity and diabetes, there is a need for new technology that is painless, non-toxic, reliable, and inexpensive enough for repetitive use to quantify long term changes in BAT metabolism in large patient studies. Microwave radiometry fits these requirements since it allows collecting thermal radiation from deep tissue non-invasively and can be calibrated to convert received power into a volume-averaged measure of absolute temperature. It has been used in medicine for noninvasive thermal monitoring of biological tissues several centimeters deep, such as breast cancer detection [10, 11], brain temperature monitoring in newborn infants [12] and adults [13], hyperthermia temperature monitoring [14, 15] and more recently vesicoureteral reflux in young children [16–18].

The present study is focused on the design and optimization of a microwave antenna capable of sensing small changes in temperature at depth as a result of increased brown fat metabolic activity, due to stimulation by cold or drugs such as norepinephrine (noradrenergic stimulation) [4, 8, 19–21]. A simplified multilayer 3D computational model, that includes BAT regions with 2–6 cm^3 below 1.5 mm skin and 3–10 mm subcutaneous fat, is used for the antenna design/optimization as well as thermal modeling of the radiometric signal.

2. METHODS

2.1 Radiometry principles

A typical MW radiometer collects thermal radiation from biological tissues using an antenna in the lower spectrum of microwaves (1–5 GHz). The MW thermal signals at the input of the radiometer are small, with spectral density of the order of 10^{-11} mW/MHz, and have to be amplified and processed by low loss and low noise MW components to retrieve the temperature of the target tissue [16, 18, 22, 23]. When connected to a radiometric receiver and loaded by a nonisothermal lossy medium (human tissue), the MW antenna will measure an equivalent temperature (T_B) determined from the weighted volumetric average temperature within the sense region of the antenna. The power collected by the antenna (P_{ant}) is directly proportional to T_B and is given by [24]:

$$P_{ant}=Gk_BT_B\Delta f \quad (1)$$

where k_B is the Boltzmann constant and G is the radiometer total gain.

Defining $T(r)$ as the physical temperature in the human tissue located at the position r within a sensing volume V, the radiometer receiver noise temperature T_{REC}, the electromagnetic interference collected by the antenna from the surrounding environment T_{EMI}, and S_{11} as the power reflection coefficient due to mismatch at the antenna/load interface, the temperature measured by the radiometer in the band Δf is given by:

$$T_B=\int_{\Delta f}\left(1-|S_{11}(f)|^2\right)\left(\int_V W(\vec{r},f)\,T(\vec{r})\,dV+T_{EMI}\right)+|S_{11}(f)|^2T_{REC}\,df \quad (2)$$

where

$$W(\vec{r},f)=\frac{P_d(\vec{r},f)}{\int_V P_d(\vec{r},f)\,dV},\quad \text{which obeys}\int_V W(\vec{r},f)\,dV=1 \quad (3)$$

$$P_d(\vec{r},f)=0.5\,\sigma(\vec{r},f)\,|E(\vec{r},f)|^2 \quad (4)$$

W is a weighting function given by the power collection pattern which, by the reciprocity theorem [24], is the same as the power density pattern P_d (W/m^3) that is a function of both electric conductivity σ (S/m) and electric field E (V/m) inside the sensing volume V. The goal of the radiometer is to retrieve target temperature $T(r)$ while reducing the contribution of the electromagnetic interference (T_{EMI}) by proper EMI shielding and low noise MW components to reduce T_{REC}. The final key element of the radiometer is the receive antenna. It is desirable to have a low mismatch (S_{11}) between the antenna and tissue load, as well as high efficiency of coupling to the target at depth, which is evaluated here in terms of the ratio of power received from the brown fat (BAT) to the total power received by the antenna:

$$\eta(f)=\frac{\int_{V_{BAT}}P_d(\vec{r},f)\,dV}{\int_V P_d(\vec{r},f)\,dV},\quad V_{BAT}\in V \quad (5)$$

2.2 Antenna design

The inherent nature of thermal noise (uniform white spectral density of the order of 10^{-21} W/Hz) implies the use of a broadband antenna to maximize power collection over frequency. In that sense, a planar microstrip log-spiral patch antenna with ground plane

backing and SMA feed structure was chosen with center frequency f_c and bandwidth Δf, since it has been proven to work for other broadband low-cost applications [12, 17, 25]. The logarithmic spiral antenna consisted of a single arm curved surface limited by edges ρ_{e1} (outer) and ρ_{e2} (inner)

$$\rho_{e1}=\rho_0 e^{a\theta}, \rho_{e2}=\rho_0 e^{a(\theta-\phi)} \quad (6)$$

where (ρ, θ) are polar coordinates, a is the spiral growth rate, and ρ_0 and $\rho_0 e^{-\varphi}$ are the initial outer and inner radius, respectively [25, 26]. Due to clinical restrictions the outermost radius of the spiral was fixed at ρ_1 = 12.5 mm and the inner radius (ρ_0 = 0.5 mm) was determined by the coaxial feed port. The end of the spiral arms were tapered (see Figure 1) to minimize reflections at lower frequencies and improve impedance matching [25]. The antenna design was implemented in HFSS™ 15 (Ansys Inc., Canonsburg, PA).

The planar log-spiral antenna presents a bidirectional radiation property [25, 26], which is not desirable for focused sensing of sub-surface brown fat. In order to exhibit a unidirectional radiation pattern, the antenna design includes a ground plane behind the spiral antenna. We choose a 175 mil hydrocarbon ceramic substrate (RO3010, Rogers Corp., USA) with dielectric constant ε_r = 10.2 and σ= 0.0022 S/m over the frequency band of interest $f_c \pm \Delta f$, that has to be determined. To improve antenna impedance match to tissue, we add a thin dielectric matching layer (coverlay) between the antenna and load (human skin), where dielectric properties and thickness (δ) are the optimization variables. Since ρ_0 and ρ_1 are constrained by allowable antenna size, the only parameter that can be optimized in the geometry of the log-spiral antenna is the number of turns (N), which is directly proportional to the spiral growth rate.

2.3 Computational model

With the antenna design and optimization parameters settled, it is necessary to define the computational model of the tissue load. Brown fat deposits can be found in the neck, mediastinum, and supraclavicular, paravertebral and suprarenal regions [20]. To exemplify human tissue in any of those regions, a multilayer 3D computational model was created using HFSS™. The multilayer model consisted of 1.5 mm skin, 3–10 mm subcutaneous (white) fat, 200 mm muscle, and an 2–6 cm^3 ellipsoid volume at the interface between subcutaneous fat and muscle to represent a variable volume of BAT (see Figure 2). The BAT ellipsoid shape and fat thickness range were chosen based on PET-CT images of the supraclavicular region [9, 19]. The correct amount of BAT in each location of the body is not yet established and BAT volumes are estimated from the literature [9, 20]. The variation in fat thickness is especially relevant since the presence of BAT is highly dependent on weight: 130 ± 98 cm^3 in lean people and 77 ± 69 cm^3 in overweight people [19].

Human thermal properties (density ρ, specific heat capacity C_p and thermal conductivity k), biological properties (metabolic heat rate Q_M and volumetric blood flow rate ω_b) and dielectric properties for f_c = 1.85 GHz (relative permittivity ε_r and electric conductivity σ) are presented in Table 1.

All tissue properties are well documented in literature except for BAT. According to CT scans, brown fat density is the same as white fat [4, 20]. Specific heat capacity and thermal conductivity of BAT are determined based on tissue water content (w) and BAT density [2, 30]:

$$C_p=4184 \cdot (0.37+0.63\, w/\rho) \quad (7)$$

$$k=0.4184 \cdot (0.133+1.36\, w/\rho) \quad (8)$$

By using equations (7) and (8) to determine thermal properties for muscle (w = 75%), skin (w = 68%) and white fat (w = 20%), the results fit into the standard deviation (SD) interval given by the thermal properties database compiled by IT'IS Foundation (Zurich, Switzerland) [27]. Brown fat thermal properties can then be estimated using w = 33% [2, 30, 31]. Dielectric properties were extrapolated from the ratio WAT/BAT in rats and the known values for WAT in humans [28, 29].

2.4 Multiphysics modeling

From Equations (2)–(4) and the reciprocity theorem [24], the received pattern of the antenna is proportional to the power deposition in the target. The electromagnetic field maintained by the antenna is calculated by solving Maxwell's wave equation, considering a time-harmonic electric field [32],

$$\nabla^2 \vec{E}\,(\vec{r}, f) + \omega^2 \mu_0 \varepsilon_0 \varepsilon_c\,(\vec{r}, f)\, \vec{E}\,(\vec{r}, f) = 0 \quad (9)$$

and using the finite element method (FEM) in HFSS™. In equation (9), ε_0 and μ_0 are free space dielectric permittivity (8.854×10^{-12} F/m) and magnetic permeability (1.257×10^{-6} N A^{-2}) respectively, $\varepsilon_c = \varepsilon_r - j\sigma/\omega\varepsilon_0$ is the complex dielectric permittivity that is modeled to be homogeneous within each medium, and ε_r is the relative permittivity of the medium. A radiation boundary condition is used in the outer domain for energy conservation. In other words, this boundary condition considers that at an infinite distance from a given source, the fields must either be vanishingly small (i.e., zero) or propagating in an outward condition [33]. Frequency dependent dielectric properties were assigned to all tissues for proper simulation of the broadband antenna [28]. This computational method has been validated experimentally in similar antennas [16, 18, 22, 23].

To complete the simulation of the theoretical power received by the antenna, it is necessary to simulate heat transfer to obtain temperature distribution. In that sense, heat transfer was simulated using another FEM simulation software, COMSOL Multiphysics® v4.2 (COMSOL, Inc., Burlington MA), which solves the bioheat equation [34, 35],

$$\rho\,(\vec{r})\, C_p\,(\vec{r})\, \frac{\partial T}{\partial t}\,(\vec{r}, t) = \nabla \cdot (k\,(\vec{r})\, T\,(\vec{r}, t)) + Q_{blood}\,(\vec{r}, t) + Q_{met}\,(\vec{r}, t) \quad (10)$$

$$Q_{blood} = \omega_b\,(\vec{r}, t)\, C_{p,b}\,(T\,(\vec{r}, t) - T_b) \quad (11)$$

where the index b stands for blood. The heat transfer in tissues described in Equation (10) is controlled by heat storage $\rho C_p \partial T/\partial t$, thermal conduction $\nabla \cdot (kT)$ that is derived from Fourier's Law, dissipation of heat through blood flow Q_{blood}, and metabolic heat rate Q_{met} (W/m^3), which is a heat source that occurs due to biochemical conversion of energy within tissue [34–36]. This model is only valid if no large vessels are nearby [35, 37].

The simulated heat transfer in the skin takes into account heat losses due to forced convection, which are represented in the boundary condition:

$$k\,(\vec{r})\, \hat{n} \cdot \nabla T\,(\vec{r}, t) = h_{air}\,(T\,(\vec{r}, t) - T_{air}) \quad (12)$$

where $\hat{n}$ is the surface normal vector of the boundary, h_{air} = 5 W/m^2/K is the convection heat transfer coefficient and T_{air} = 25 °C is the room temperature in thermoneutral conditions. Continuity conditions were assigned at the interface antenna/skin.

The goal of the radiometric antenna sensor is to monitor brown fat metabolism which can be excited from its baseline using cold or noradrenergic stimulation [8, 19, 20, 38]. The phenomenon of increased metabolic activity is not yet fully defined, but indications to date suggest that BAT metabolism increases up to 15-fold [5] in humans and perhaps as much as 50-fold in rats [38]. We will present cases for 5, 10, 15, 20 and 25 fold increases in metabolic activity and take into account that blood perfusion will follow 94% of this increase due to thermoregulation [6]. Cold exposure induces vasoconstriction, which in turns reduces blood flow [9]. A 60 % reduction in blood perfusion and metabolism is assumed during cold exposure (15 °C) [39].

3. RESULTS

3.1 Antenna optimization

Figure 3 shows the antenna reflection coefficient of the tapered log-spiral antenna over 0.5–3 GHz for substrate (Figure 3a) and coverlay (Figure 3b) permittivity, number of log spiral turns (Figure 3c) and coverlay thickness (Figure 3d). The tissue load has 1.5 mm skin, 3 mm fat and a BAT volume of 6 cm^3. The vertical marker lines at 850 MHz, 1.85 GHz and 2.4 GHz represent center frequencies allocated by the Federal Communications Commission (FCC) to pagers, wireless LAN, mobile phones and pagers that can be found in hospital settings. Ideally, reception at these frequencies can be shielded or filtered to minimize EMI contamination of the radiometric signal [40]. All signals present good reflection coefficients (S_{11}<-10dB) over a wideband (1.4 GHz – 2.5 GHz) as typical of log-spiral antennas. The criteria to choose the wideband was however based on a better impedance match range (S_{11}<-13dB) as presented by the horizontal marker, and as a result the chosen frequency band is (1.5 GHz – 2.2 GHz)

Within all parametric simulations, only the ceramic substrate permittivity (see Figure 4) shifted the maximum antenna efficiency towards lower frequencies (1–2 GHz), which presented better impedance match results. However, very thick substrates of high dielectric low-loss material are currently of limited availability for low-cost manufacturing, and there is no significant improvement in targeted power detection unless the substrate dielectric constant is notably above 30.

Figure 5 shows the volume loss density pattern (W/m^3) simulated in HFSS™ with nominal values (N = 2.25, $\delta_{coverlay}$ = 1 mm, $\varepsilon_{r,coverlay}$ = 30 and $\varepsilon_{r,substrate}$ = 10.2).

3.2 Thermal modeling of BAT metabolism

Steady-state thermal simulations were performed in COMSOL® to address two distinct scenarios: cold and noradrenergic stimulation. The mesh in the heat transfer model was refined until solutions presented energy conservation and mesh independence. The simulated temperature distribution and the electromagnetic simulations were combined [Equations (1) and (2)] to compute the theoretical power received by the antenna. The receiver temperature T_{REC} = 95 K was taken from literature as a typical value for low noise radiometric systems [41]. Figure 6 shows the average temperature increase in BAT region as a consequence of the increased BAT metabolism induced by cold stimulation and noradrenergic stimulation.

Figure 7 and Figure 8 show the theoretical radiometric power variation (ΔP_{ant}) as a function of metabolism change (W/m^3) for cold and noradrenergic stimulation, respectively. In either case the average simulated power is −86.74 ±0.03 dBm. Accounting for the 1st stage (+15

dB) and 2nd stage (+40dB) gain as well as −5 dB loss in the microwave components and interconnects, the expected power collected by the radiometer is around −36.74 ±0.03 dBm, which corresponds to 0.21μW. As the BAT is activated by cold or norepinephrine, the power received changes of few thousandths of dB above the baseline value. Thus the radiometric systems must be stable enough to detect 50 pW changes in power.

The radiometric sensitivity presented in Figure 7 and Figure 8 is achievable with current MW radiometry and is in accordance with recent measurements using similar radiometers in our group [13].

4. DISCUSSION

By combining electromagnetics and heat transfer analysis, a new computational model was established to simulate power emitted from activated human brown fat and received by a broadband antenna on the tissue surface. The model is based on the Plank's principle that thermal energy radiates from living tissue with a measurable amount of power in the microwave frequency band. This thermal radiation can be collected with a microwave receive antenna, amplified, filtered and quantified with a sensitive power detector. With appropriate electronics and software processing, the received power can be correlated directly with temperature of tissue located within the radiation field of the antenna. Such a measurement device is termed a microwave radiometer. The design and optimization of a radiometric antenna based on tapered log-spiral geometry is the subject of this study. Once the design is established, thermal modeling and radiometry principles will determine the feasibility for brown fat monitoring with a compact microwave radiometer.

The parametric analysis presented in Figure 3 provides a basis for determining the best frequency band for proper impedance match and the ones to avoid due to EMI. The best compromise between good match impedance (S_{11}<-13dB) and avoiding regions with EMI is found in the frequency band 1.5 GHz – 2.2 GHz for $N = 2.25$, $\delta_{coverlay} = 1$ mm, $\varepsilon_{r,coverlay} = 30$ and $\varepsilon_{r,substrate} = 10.2$ (nominal values), which presents a wideband $\Delta f = 700$ MHz as desired. However, within this band there is a frequency allocated for wireless devices (1.85 GHz). This frequency can be eliminated using a notch filter in the radiometer electronics. In this scenario the antenna's frequency band would became $\Delta f = 650$ MHz, which is still considered a broadband. Regarding to permittivity parameterizations, the higher permittivity values of both substrate and coverlay could improve the power collection over a wider band. However, we are limited in manufacturing to the best available materials, which currently have $\varepsilon_r = 30$ and $\varepsilon_r = 10.2$ for coverlay and substrate, respectively.

In antenna design, the optimal impedance match does not guarantee best efficiency in collecting power from a specific target at depth and Figure 4 is a clear example. The parametric optimization for all parameters (N, $\delta_{coverlay}$, $\varepsilon_{r,coverlay}$ and $\varepsilon_{r,substrate}$) was implemented, but only the ceramic substrate permittivity changed significantly the optimization function. In terms of efficiency, the best frequency band ($\varepsilon_{r,substrate} = 30$) would be 2.2– 3.0 GHz. However, this band presents a poor impedance match and substrate permittivity much larger than 10 are currently not available for low-cost standard circuit manufacturing. Besides these two limiting factors, there is an EMI band at 2.4 GHz. At this point a compromise must be established and since the band 1.5–2.2 GHz presents an average 19% efficiency, meaning that 19% of power will be collected from the BAT region, the chosen optimal frequency band remained 1.5–2.2 GHz.

The first key element in the radiometric formula [Equation (1)] is the received pattern from the target model. From the reciprocity theorem the power deposition and the received pattern by the radiometric antenna are the same. From Figure 5 it is clear that BAT is lossier

than WAT, and the higher absorption enhances the power collection from BAT even at depth (11.5 mm from the surface to the center of BAT ellipsoid). The second key element is temperature distribution, which was computed in COMSOL®. In this heat transfer model, the mesh was refined until solutions presented energy conservation and mesh independence. Figure 6 shows the average increased temperature in the BAT region where, for all scenarios (2–6 cm^3 BAT volume and 3–10 mm WAT thickness), the increased temperature range was 0.33–1.47 °C. To retrieve power, the deposition pattern was imported from mesh points in HFSS™ to COMSOL®, where it was linearly interpolated and combined with 3D temperature maps. The average power received by the surface antenna was −86.74 dBm, when considering no gain. Taking into consideration that our radiometer [13] presents a 15 dB gain in the 1st stage, 40 dB in the 2nd stage, and 5 dB of losses in the MW components and interconnections [41], the expected power after amplification is −36.74 dBm, which is similar to previous experimental measurements in monitoring temperature of kidney and brain [13, 22] and can be detected with commercially available microwave power detectors.

From Figure 7 it is clear that the theoretical radiometric power is dependent on BAT metabolism (W/m^3), in particular when stimulated by mild cold (15 °C). For metabolic rates $Q_M > 40\times10^3$ W/m^3, the radiometric power tends to become independent of metabolic activity, but so far literature only describes variations up to 15-fold [5], which is equivalent to 38.7×10^3 W/m^3 on Figure 7. The minimum radiometric power variation is 2.2 mdBm for 5-fold BAT metabolism increase (2 cm^3 BAT volume below 10 mm WAT thickness), which is detectable using recent microwave radiometry calibration and stabilization techniques [13, 22]. The radiometric detectability might even be more significant if the stimulus becomes more pronounced, e.g. maintaining 5–10°C air temperature.

The noradrenergic stimulation in Figure 8 does not produce radiometric power changes as significant as the cold stimulation. The worst case scenario (2 cm^3 BAT volume below 10 mm WAT thickness) produced only a 1.2–2.5 mdBm increase of radiometric power from 5 to 25 fold increase in metabolic activity. Because radiometric system intrinsic noise is around1 mdBm, only the higher part of that range can be detected. However, for this particular application the integration time may be extended to several minutes and even hours, since the goal is monitoring of long term changes and not detection of short transient changes such as the rapid exposure to cold environment. Increasing the integration time will offer a significant reduction in noise level. The higher radiometric power variation verified under cold stimulus is related to the fact BAT region becomes significantly hotter than its surrounding due to vasoconstriction induced by cold in the surrounding tissues. In the absence of cold, and when a drug is targeted to BAT, the gradient between this region and its surrounding tissues is significantly reduced since no vasoconstriction occurs.

This work addresses theoretical modeling of temperature distributions around small depots of BAT at depth. PET-CT images were used to establish realistic volumes, shapes, and locations of BAT. We used 2–6 cm^3 BAT volumes since we believe these represent worst case scenarios. BAT is often found concentrated in the supraclavicular region. 2D PET/CT scans indicate volumes up to 20 cm^3 in lean people and approximately half for overweight people. The next step in this project will involve accurate segmentation of brown fat depots and surrounding tissues for different BMI groups, as soon as better images become available. Experimental validation of both antenna and thermal models will be performed, similar to the work completed previously for this deep penetrating log spiral antenna in kidney and brain tissues [16, 22, 23, 42].

5. CONCLUSIONS

We presented a mathematical model that allows studying the feasibility of non-invasive brown fat monitoring using microwave radiometry. The chosen sensor is based on a tapered log-spiral antenna: its design and operating frequency band were selected based on maximizing the ratio of power received by the radiometric antenna from the target at depth, maximizing impedance match to skin, and minimizing overlap with allocated wireless communications frequencies. The optimized frequency band was 1.5–2.2 GHz, with an average antenna efficiency of 19%. These characteristics proved to be enough to detect small temperature changes (0.5 °C) in the BAT region, located up to 12 mm deep. When using cold stimulus the radiometric power sensitivity was more pronounced. In conclusion, the developed miniature radiometric antenna sensor appears suitable for low-cost non-invasive long term monitoring of BAT metabolism.

Acknowledgments

The authors would like to acknowledge support from NIH R21-DK092912. We would like to acknowledge software support from ANSYS, Inc. and COMSOL, Inc. Dário B. Rodrigues acknowledges the Portuguese Foundation for Science and Technology (FCT-MEC) for a post-graduate scholarship SFRH/BD/73215/2010. The authors also acknowledge partial funding from the Portuguese research grant PEst-OE/FIS/UI0068/2011 through FCT-MEC.

REFERENCES

[1]. Hossain P, Kawar B, El Nahas M. Obesity and diabetes in the developing world--a growing challenge. N Engl J Med. 2007; 356(3):213–5. [PubMed: 17229948]

[2]. Hu HH, Perkins TG, Chia JM, et al. Characterization of human brown adipose tissue by chemical-shift water-fat MRI. AJR. American journal of roentgenology. 2013; 200(1)

[3]. Cannon B, Nedergaard J. Brown adipose tissue: function and physiological significance. Physiol Rev. 2004; 84(1):277–359. [PubMed: 14715917]

[4]. Cypess AM, Lehman S, Williams G, et al. Identification and importance of brown adipose tissue in adult humans. N Engl J Med. 2009; 360(15):1509–17. [PubMed: 19357406]

[5]. Virtanen KA, Lidell ME, Orava J, et al. Functional brown adipose tissue in healthy adults. N Engl J Med. 2009; 360(15):1518–25. [PubMed: 19357407]

[6]. Muzik O, Mangner TJ, Granneman JG. Assessment of oxidative metabolism in brown fat using PET imaging. Frontiers in endocrinology. 2012; 3

[7]. Lunati E, Marzola P, Nicolato E, et al. In vivo quantitative lipidic map of brown adipose tissue by chemical shift imaging at 4.7 tesla. Journal of Lipid Research. 1999; 40(8)

[8]. Rothwell NJ, Stock MJ. A role for brown adipose tissue in diet-induced thermogenesis. Nature. 1979; 281(5726):31–5. [PubMed: 551265]

[9]. Lee P, Ho KKY, Greenfield JR. Hot fat in a cool man: infrared thermography and brown adipose tissue. Diabetes Obesity & Metabolism. 2011; 13(1):92–93.

[10]. Carr KL. Microwave Radiometry - Its Importance to the Detection of Cancer. IEEE Transactions on Microwave Theory and Techniques. 1989; 37(12):1862–1869.

[11]. Bardati F, Iudicello S. Modeling the visibility of breast malignancy by a microwave radiometer. IEEE Trans Biomed Eng. 2008; 55(1):214–21. [PubMed: 18232364]

[12]. Hand JW, Van Leeuwen GMJ, Mizushina S, et al. Monitoring of deep brain temperature in infants using multi-frequency microwave radiometry and thermal modelling. Physics in Medicine and Biology. 2001; 46(7)

[13]. Stauffer, P.; Salahi, S.; Rodrigues, D., et al. Stable microwave radiometry system for long term monitoring of deep tissue temperature. SPIE; San Jose CA, USA: 2013.

[14]. Jacobsen S, Stauffer PR. Can we settle with single-band radiometric temperature monitoring during hyperthermia treatment of chestwall recurrence of breast cancer using a dual-mode

transceiving applicator? Physics in Medicine & Biology. 2007; 52(4):911–28. [PubMed: 17264361]

[15]. Dubois L, Sozanski JP, Tessier V, et al. Temperature control and thermal dosimetry by microwave radiometry in hyperthermia. IEEE Transactions on Microwave Theory and Techniques. 1996; 44(10, pt.2):1755–61.

[16]. Arunachalam K, Maccarini P, De Luca V, et al. Modeling the detectability of vesicoureteral reflux using microwave radiometry. Phys. Med. Biol. 2010; 55(18):5417–35. [PubMed: 20736499]

[17]. Snow BW, Arunachalam K, De Luca V, et al. Non-invasive vesicoureteral reflux detection: Heating risk studies for a new device. Journal of Pediatric Urology. 2011; 7(6)

[18]. Stauffer, P.; Maccarini, P.; Arunachalam, K., et al. Microwave Radiometry for Non-Invasive Detection of Vesicoureteral Reflux (VUR) Following Bladder Warming. SPIE Press; Bellingham WA: 2011. PMCID:3409575

[19]. Lichtenbelt, W. D. v. M.; Vanhommerig, JW.; Smulders, NM., et al. Cold-Activated Brown Adipose Tissue in Healthy Men. New England Journal of Medicine. 2009; 360(15):1500–1508. [PubMed: 19357405]

[20]. Nedergaard J, Bengtsson T, Cannon B. Unexpected evidence for active brown adipose tissue in adult humans. American Journal of Physiology-Endocrinology and Metabolism. 2007; 293(2):E444–E452. [PubMed: 17473055]

[21]. Nechad M, Nedergaard J, Cannon B. Noradrenergic stimulation of mitochondriogenesis in brown adipocytes differentiating in culture. American Journal of Physiology. 1987; 253(6):C889–C894. [PubMed: 2827500]

[22]. Arunachalam K, Maccarini P, De Luca V, et al. Detection of vesicoureteral reflux using microwave radiometry-system characterization with tissue phantoms. IEEE Trans Biomed Eng. 2011; 58(6):1629–36. [PubMed: 21257366]

[23]. Birkelund Y, Klemetsen O, Jacobsen SK, et al. Vesicoureteral reflux in children: a phantom study of microwave heating and radiometric thermometry of pediatric bladder. IEEE Trans Biomed Eng. 2011; 58(11):3269–78. [PubMed: 21900069]

[24]. Balanis, C. Antenna Theory: Analysis and Design. John Wiley & Sons, Inc.; Hoboken, New Jersey: 2005.

[25]. Thaysen J, Jakobsen K, Appel-Hansen J. A logarithmic spiral antenna for 0.4 to 3.8 GHz. Applied Microwave & Wireless. 2001

[26]. Dyson J. The Equiangular Spiral Antenna. IRE Transactions on Antennas Propagation. 1959; AP-7:181–187.

[27]. Hasgall, P.; Neufeld, E.; Gosselin, M., et al. IT'IS Database for thermal and electromagnetic parameters of biological tissues. 2011. www.itis.ethz.ch/database

[28]. Gabriel, C. Compilation of the dielectric properties of body tissues at RF and microwave frequencies. Texas (USA): 1996.

[29]. TopSakal E, Colebeck E, Rodrigues D, et al. Brown and white fat dielectric properties in rats. Physics in Medicine and Biology, Under Review. 2013

[30]. Takata, A.; Zaneveld, L.; Richter, W. Laser-induced thermal damage in skin. USAF School Aerospace Medicine, Brooks AFB; TX: 1977.

[31]. Dubinskaya VA, Eng LS, Rebrow LB, et al. Comparative study of the state of water in various human tissues. Bulletin of Experimental Biology and Medicine. 2007; 144(3)

[32]. Balanis, CA. Advanced Engineering Electromagnetics. Wiley; New York: 1989.

[33]. Pozar, DM. Microwave Engineering. John Wiley & sons, Inc.; New York: 1998.

[34]. Wissler EH. Pennes' 1948 paper revisited. Journal of Applied Physiology. 1998; 85:36–42.

[35]. Pennes HH. Analysis of tissue and arterial blood temperatures in the resting human forearm. Journal of Applied Physiology. 1948; 1(2):93–122. [PubMed: 18887578]

[36]. Song, C.; Choi, I.; Nah, B., et al. Microvasculature and perfusion in normal tissues and tumors. Springer-Verlag; Berlin, New York: 1995.

[37]. Fan J, Wang L. Analytical theory of bioheat transport. Journal of Applied Physics. 2011; 109(10)

[38]. Cypess AM, Lehman S, Williams G, et al. Identification and Importance of Brown Adipose Tissue in Adult Humans. New England Journal of Medicine. 2009; 360(15):1509–1517. [PubMed: 19357406]

[39]. Vuksanovic V, Sheppard LW, Stefanovska A. Nonlinear relationship between level of blood flow and skin temperature for different dynamics of temperature change. Biophysical Journal. 2008; 94(10):L78–L80. [PubMed: 18339767]

[40]. LaSorte, NJ.; Barnes, WJ.; Refai, HH., et al. Characterization of the Electromagnetic Environment in a Hospital and Propagation Study. Emc 2009: Ieee International Symposium on Electromagnetic Compatibility; 2009. p. 135-140.Technical Paper

[41]. Klemetsen O, Birkelund Y, Jacobsen SK, et al. Design of Medical Radiometer Front-End for Improved Performance. Prog Electromagn Res B Pier B. 2011; 27:289–306. [PubMed: 21779411]

[42]. Stauffer, P.; Maccarini, P.; Arunachalam, K., et al. Microwave Radiometry for Non-Invasive Detection of Vesicoureteral Reflux (VUR) Following Bladder Warming. SPIE Press; Bellingham WA: 2011.

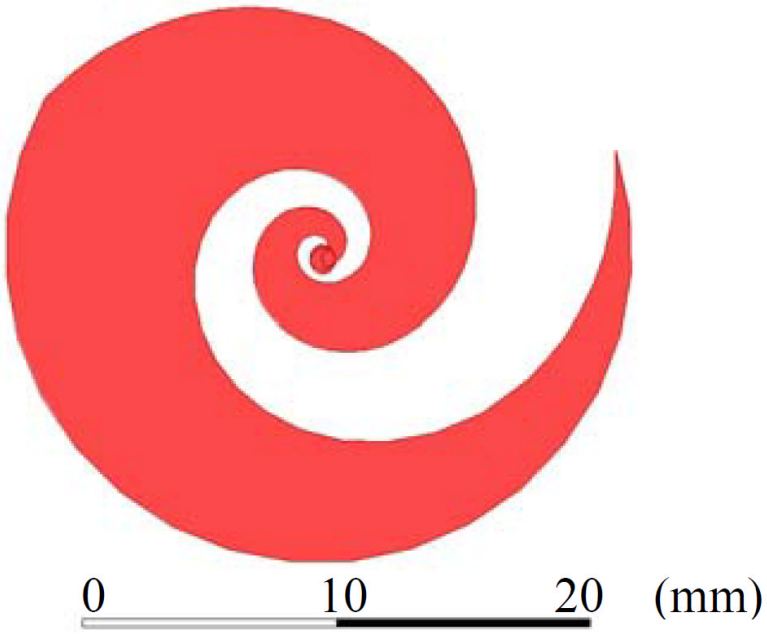

Figure 1.
Microstrip log-spiral patch antenna design with tapered ends.

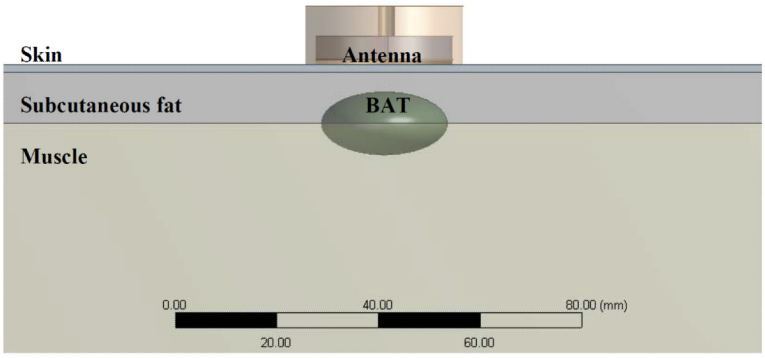

Figure 2.
Zoomed-in and lateral view of the 3D multiphysics computational model of multilayer human body: skin, subcutaneous white fat, brown fat (BAT) and muscle.

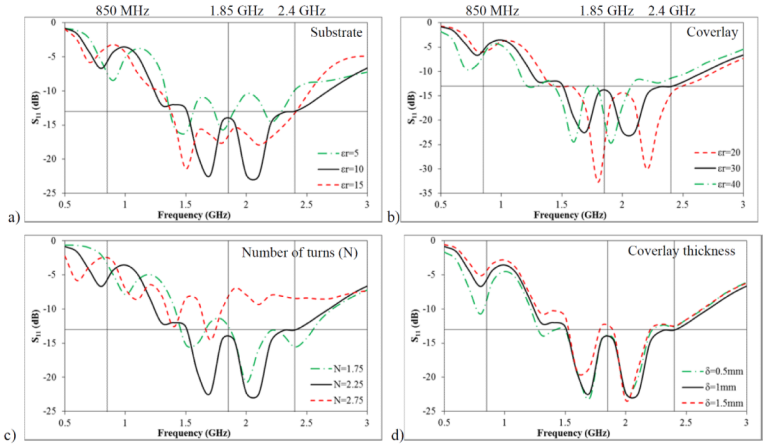

Figure 3.

Parametric simulations to improve impedance matching at the interface between antenna and load. a) S_{11} vs. substrate relative permittivity; b) S_{11} vs. coverlay relative permittivity; c) S_{11} vs. number of log-spiral turns and d) S_{11} vs. coverlay thickness. Nominal values: N = 2.25, $\delta_{coverlay}$ = 1 mm, $\varepsilon_{r,coverlay}$ = 30 and $\varepsilon_{r,substrate}$ = 10.2.

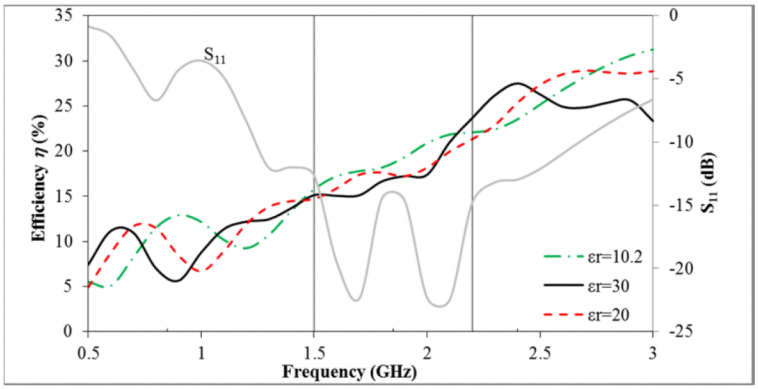

Figure 4.
Parametric simulations on the substrate relative permittivity to improve the ratio of power received from BAT.

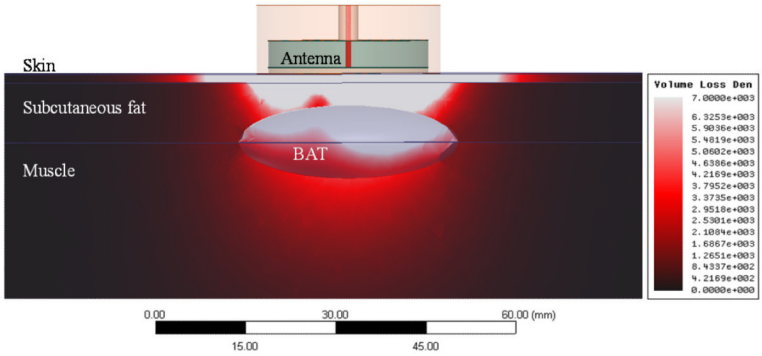

Figure 5.

Simulated volume loss density (W/m^3) for a 1W source at the antenna input in the computational domain (lateral view) for 10 cm thickness of subcutaneous fat and a BAT volume of 6 cm^3.

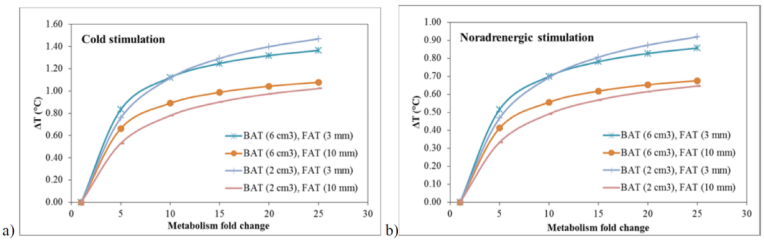

Figure 6.

Average temperature increase in BAT region due to increased BAT metabolism induced by cold stimulation (a) and noradrenergic stimulation (b); BAT volumes (cm^3) and WAT thickness (mm) are presented.

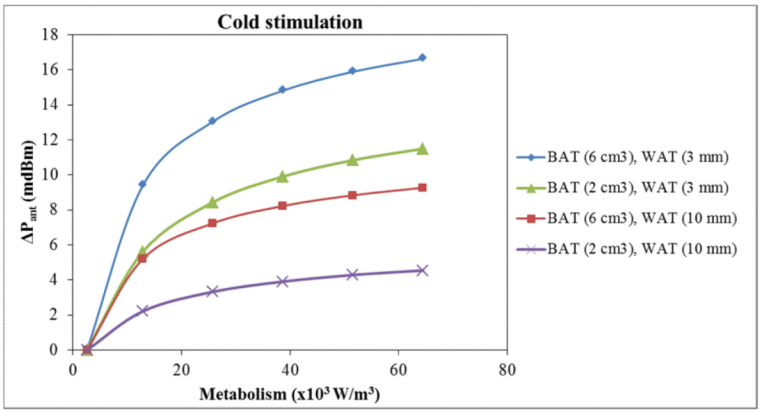

Figure 7.
Parametric simulations to assess antenna's sensitivity to metabolic variations under mild cold simulation (15 °C); BAT volumes (cm^3) and WAT thickness (mm) are presented.

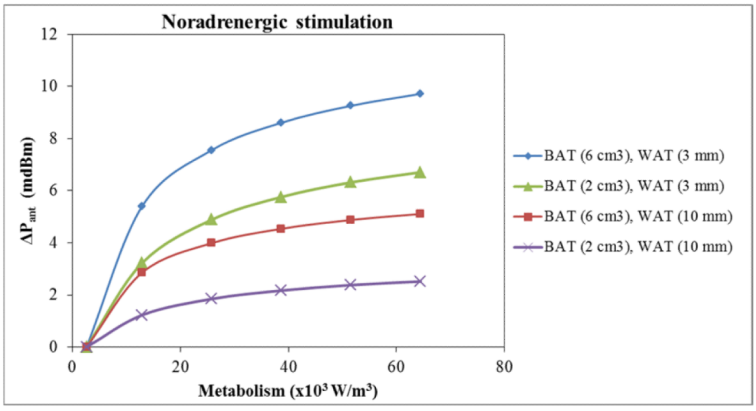

Figure 8.
Parametric simulations to assess antenna's sensitivity to metabolic variations under noradrenergic simulation; BAT volumes (cm^3) and WAT thickness (mm) are presented.

Table 1

Design properties for human tissues and antenna constituents: thermal properties [6, 27], biological properties [27] and dielectric properties at 1.85 GHz [28, 29].

Property / **Tissue**	ρ (kg/m^3)	C_p (J/kg/K)	k (W/m/K)	Q_M (W/m^3)	ω_b (kg/s/m^3)	σ (S/m)	ε_r
Skin	1109	3391	0.37	1827	2.064	1.257	43.765
White fat	911	2127	0.18	462	0.521	0.080	5.344
Brown fat	911	2503	0.26	2579	1.221	0.484	8.742
Muscle	1090	3421	0.49	1052	0.746	1.368	53.484